Magnetic Resonance Imaging 57 (2019) 243–249

Contents lists available at ScienceDirect

Magnetic Resonance Imaging

journal homepage: www.elsevier.com/locate/mri

Original contribution

Reproducibility of inhomogeneous magnetization transfer (ihMT): A test-retest, multi-site study

Lei Zhang[a], Tao Chen[a], Hongzhe Tian[a], Hongqiang Xue[a], Huipeng Ren[a], Li Li[a], Qing Fan[a], Baohong Wen[b], Zhuanqin Ren[a,*]

[a] Department of Radiology, Baoji Center Hospital, Baoji, Shaanxi, People's Republic of China
[b] Department of Radiology, Zhengzhou University First Affiliated Hospital, Zhengzhou, Henan, People's Republic of China

ARTICLE INFO

Keywords:
ihMT
Reproducibility
Myelin imaging

ABSTRACT

Background: Inhomogeneous magnetization transfer (ihMT) has been reported to feature superior sensitivity and specificity for myelin imaging. However, the reproducibility on ihMT has yet been rarely investigated up to date. The purpose of the present study is to assess the multi-center reproducibility and test-retest variability of ihMT in central nervous system.

Methods: 5 volunteers were recruited and scanned twice on three 3.0 T magnetic resonance imaging (MRI) scanners using ihMT with identical scan parameters. The maps of quantitative ihMT (qihMT) and ihMT ratio (ihMTR) for each scan were calculated. Voxel based analysis then was performed to generate qihMT and ihMTR values for major white matter fibers. The intra- and inter-scanner reliability and reproducibility was assessed with intraclass correlation coefficients (ICCs). Bland-Altman method was used to show the level of agreement between two measurement types. Paired *t*-test and one-way ANOVA test were also used to compare the difference between inter- and intra-scanner, respectively.

Results: In the 10 major white matter tracts areas, the ICCs indicated high intra- and inter-scanner measurement reliability and reproducibility. The Bland-Altman plots together with 95% confidence interval (CI) across all ROIs in the five volunteers also demonstrated good repeatability. No significant inter- and intra-scanner differences were found in Paired *t*-test and one-way ANOVA tests.

Conclusion: Good inter- and intra-scanner reliability and reproducibility of ihMT measurements were observed in this study. These findings support the use of ihMT measurements as biomarkers in multicenter and/or longitudinal studies.

1. Introduction

Discovered in 1854 by Rudolf Virchow, the lipid-rich substance of myelin was found to mainly exist in white matter that surrounds the axon of nerve cells, forming an electrically insulating layer. Myelin sheath is analogous to the layer of plastic insulation surrounding an interior wire that is the nerve. The main purpose of the myelin sheath is to increase the speed at which impulses propagate along the myelinated fiber. The myelin sheath also assures the electrical current travel without being corrupted or scrambled. [1] Alteration of myelination is a hallmark of many central nervous system diseases including multiple sclerosis [2,3], phenylketonuria [4,5], schizophrenia [6], epilepsy [7], psychotic disorders [8], and Alzheimer's disease [9]. It is also a recognized as a biomarker of brain development [10].

Assessment of myelin content is usually performed in post-mortem study. MRI, due to its non-invasive nature, relative high spatial imaging resolution and excellent soft tissue contrast, has been widely used for the imaging of myelin. Various MR imaging techniques for in-vivo myelin assessment have been proposed and validated. Fractional anisotropy (FA) derived from diffusion tensor imaging (DTI) may quantifies diffusion directional dependency, and has been reported to be sensitive to changes in myelin content [11]. However, DTI measures can be affected by several factors besides myelination, such as axon density, caliber, cell swelling, fiber architecture and myelin thickness [12]. Another technique, which is termed as multicomponent-driven equilibrium single-component observation of T1and T2 (mcDESPOT) model, combines spoiled gradient echo (SPGR) and balanced steady-state free precession (bSSFP) imaging to produce a three-pool tissue model, including volume fractions for intra/extracellular, free, and myelin-bound water (VFm) [13]. Compared to FA, VFm is insensitive to

* Corresponding author at: Department of Radiology, Baoji Center Hospital, No. 8 Jiang Tan Road, Baoji 721008, Shaanxi, People's Republic of China.
E-mail address: Renzhuanqin@163.com (Z. Ren).

https://doi.org/10.1016/j.mri.2018.11.010
Received 2 August 2018; Received in revised form 29 October 2018; Accepted 17 November 2018

other tissue properties affecting T2 relaxation times. However, VFm may still be affected by magnetization transfer effects and field inhomogeneity [14]. On the other hand, magnetic transfer (MT) effects of protons bound to large macromolecules; under the assumption that most of the macromolecular content in the CNS is myelin, the MT effect can thus be exploited as an indirect assessment of myelin content. Strong correlation has been reported between MT ratio and density of myelin both in rat brains [15] and post mortem human brains [16]. However, MT measurement may be influenced by tissue inflammation or sequence-dependent parameters such as pre-pulse frequency [17]. Also, quantification of MT effects is confounded by many factors and is still under investigation [18].

Recently Varma et al. reported a myelin specific version of MT, which was termed as inhomogeneous magnetization transfer (ihMT). Compared to MT, ihMT allows imaging of the specific MT effects arising from inhomogeneously broadened components of the NMR spectrum, which is assumed to be mainly contributed by myelin [19]. In vivo experiments have demonstrated the sensitivity and specificity of ihMT in discriminating between myelinated and other tissues [20]. A recent study comparing ihMT, DTI and mcDESPOT reported that all three measurements appear to be sensitive to myelin content, though qihMT from ihMT and VFm from mcDESPOT appear to be more specific to it than RD from DTI [21].

The assessment of myelin content, whether for brain development or disease progression, often involves multiple center collaboration or longitudinal data collection. Hence reproducibility and inter-observer variability of the ihMT quantification is crucial for its widespread clinical applications. The reproducibility of traditional myelin imaging techniques has been previously demonstrated [22–24]. However, reproducibility study on ihMT was rarely reported. To our knowledge, there is only one study reported up to date: Mchinda et al. [25] assessed the reproducibility of ihMT with 3 volunteers scanned twice on a 1.5 T system, which is limited in its scope. The purpose of the present study is to assess the multi-center reproducibility and test-retest variability of ihMT in central nervous system on 3 T systems, by evaluating ihMT derived parameters of major tract areas in white matter.

2. Materials and methods

2.1. Subjects

This study was approved by local ethics committee and written informed consents were obtained from all subjects prior to MRI examinations. Between Oct 2017 to Feb 2018, data collections were performed on five healthy young volunteers (age from 24 to 33 years, 2 females and 3 males) without a history of neurological diseases.

2.2. Data acquisition

All experiments were conducted on a 3 T MR system (Discovery MR750, GE Healthcare, Waukesha, USA) equipped with an 8 channels head coil. All subjects received 3D T1 and ihMT scan. T1 data were acquired using an inversion recovery 3D spoiled gradient echo (SPGR) sequence with the following parameters: TR/TE: 8.2/3.2 ms, inversion recovery time 450 ms, Flip angle 12°, parallel imaging factor 2, 24 cm field of view, matrix 256 ∗ 256, 1 mm slice thickness, 184 axial slices covering the whole brain and the scan time was 4:35. The ihMT images were acquired using a 3D SPGR sequence with different MT preparation pulses. Detailed parameters are as following: TR/TE = 10.3 ms/2.1 ms, 23 cm field of view, matrix 96 × 96, sagittal plane, 56 slices, flip angle 8°. The sequence included a 5 ms Fermi preparation pulse with peak B1 of 45 mG and 5 kHz offset prior to each excitation. The frequency of MT preparation pulses cycled between positive offset (+5 kHz), first dual offset (±5 kHz), negative offset (−5 kHz), and second dual offset. The cycle repeated 6 times for SNR consideration. For quantification purpose, 2 extra reference datasets were acquired without MT preparation: one with 8° flip angle and another with 32° flip angle. The total scan time was 5:14.

In order to assess the multi-center reproducibility of ihMT, data acquisitions of all subjects were performed at three different centers equipped with the same scanner platform and receive coils; to assess the test-retest variability of the measurements, all subjects were scanned twice at two-time points (3 days to 45 days between two scans) on each scanner. All ihMT scans were performed with the same acquisition parameters and subjects' position.

2.3. ihMT calculation

The original acquired ihMT images are processed with a post-processing software provided by GE Healthcare. Two quantitative measures, quantitative ihMT (qihMT) and ihMT ratio (ihMTR), were derived using the model below [19,21].

$$qihMT = R1_{dual} - R1_{+/-} = \frac{c\alpha^2}{2TR} S_c \left(\frac{1}{S_+ + S_- - S_{dual1} - S_{dual2}} \right) \quad (1)$$

$$ihMTR = \frac{S_+ + S_- - S_{dual1} - S_{dual2}}{S_b} \quad (2)$$

where S_+, S_-, S_{dual1} and S_{dual2} are the measured signal intensity of positive, negative, first and second dual frequency offset during MT state, S_b is baseline signal of 8° flip angle reference state and S_c is signal from the 32° high flip angle reference state. c = 4 is a flip angle scale factor between the excitation angle of the MT and reference conditions, α = 8 is the flip angle in MT state. R1 is the average longitudinal relaxation rate from repetitions of an MT state (either dual frequency or single frequency), qihMT is approximated by Δ(R1) and describes the difference in longitudinal relaxation rates between these two states.

2.4. Image processing

The anatomical images were first co-registered to the MT reference images. Registered structural images were then nonlinearly transformed into the ICBM 152 T1 template in the Montreal Neurological Institute (MNI) space using FSL. The inverse transformations were used to warp the JHU-ICBM 2 mm atlas from the MNI space to the MT reference native space. Discrete labeling values were preserved using a nearest-neighbor interpolation method. Masks of 10 major white matter fibers in the individual space were obtained following the above procedure: Genu of corpus callosum, Body of corpus callosum, Splenium of corpus callosum, Corticospinal tract, Cerebral peduncle, Limb of internal capsule, Corona radiata, Posterior thalamic radiation, Cingulate gyrus and Hippocampus. The mean values of qihMT and ihMTR were then extracted from the white matter mask in each subject. A detailed illustration of image processing can be found in Fig. 1.

2.5. Statistical analysis

All data is expressed as mean ± standard deviation (SD). The average values of qihMT and ihMTR for each volunteer were used for quantitative statistical analyses. Normality was analyzed using the Kolmogorov-Smirnov test, with both qihMT and ihMTR revealing approximately normal distribution. The intra- and inter-scanner reliability and reproducibility was assessed with intraclass correlation coefficients (ICCs), which measures the ability of a method to detect differences between subjects consistently. ICC values ranges between 0 and 1 and close to 1 indicate high reliability. A two-way random average-measure ICC values were calculated in this study. Bland-Altman method was also used to compare two measurements and can be used to show the level of agreement between two measurement types. The coefficient of repeatability values was calculated as 2 times the SD of differences between two measurements and was used to create Bland-Altman plots. Paired *t*-test and one-way ANOVA test were used to compare the

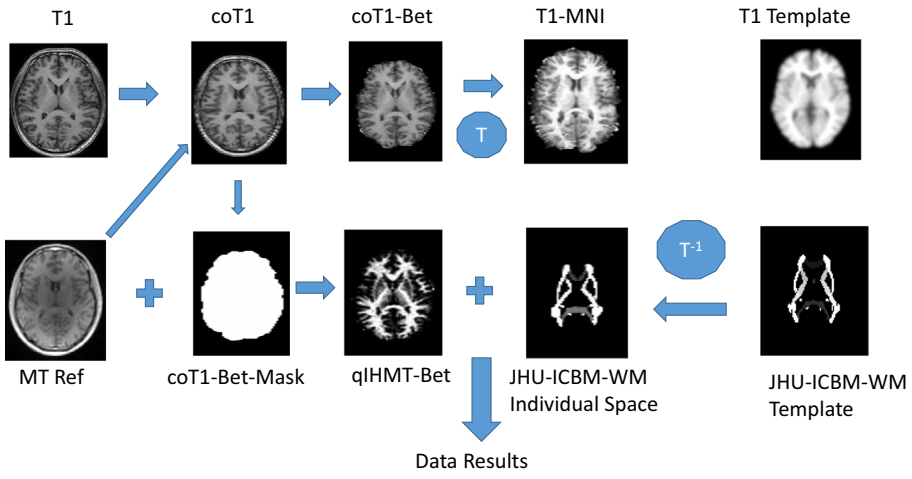

Fig. 1. Illustration of data analysis process. Step1: the acquired T1 is co-registered to MT reference images (coT1). Step2: Skulls are then removed from T1 (coT1-Bet) and qihMT (qihMT-Bet) using brain extraction tool. Step 3: coT1-Bet is transferred from individual space to MNI space (T1-MNI). Transform matrix is generated in this step. Step4: Inverse transform of JHU-ICBM white matter template from MNI space to individual space (JHU-ICBM-WM Individual Space). Mask of different white matter tracts can be generated using the template. Step5: Combining qihMT-Bet and the generated masks, data results of qihMT (as well as ihMTR) of different tracts can be calculated.

difference between inter- and intra-scanner, respectively. All statistical analysis was performed with software (SPSS v. 19.0, Chicago, IL) and $P < 0.05$ was set as statistical significant.

3. Results

Post processed ihMT images of one typical subject at two-time points at three sites were shown in Fig. 2. Similar morphological and quantitative ihMT values from different time points and different centers can be observed.

A summary of the mean value and standard deviation (SD) of qihMT and ihMTR of ten areas were shown in Tables 1 and 2. The ICCs of the same areas of qihMT and ihMTR values between intra- and inter-scanner were listed in Table 3. In general, in these ten areas, the ICCs had high intra- and inter-scanner measurement reliability and reproducibility. The agreement was highest for qihMT values of posterior thalamic radiation between 1st and 3rd scanner (ICC, 0.948; 95% confidence interval [CI], 0.901–0.995) and lowest for ihMTR values of corona radiata between 2nd and 3rd scanner (ICC, 0.711; 95% CI, 0.675–0.746).

The Bland-Altman plots together with 95% confidence interval (CI) of intra- and inter-scanner qihMT and ihMTR measurements across all ROIs in the five volunteers were shown in Fig. 3. The scatter plot of average values of qihMT and ihMTR on three scanners were shown in Fig. 4. All these figures showed good repeatability between intra- and inter-scanner and was considered clinically acceptable.

Paired *t*-test and one-way ANOVA test were used to compare the difference between inter- and intra-scanner difference for qihMT and ihMTR. Results of paired *t*-test one-way ANOVA analysis are listed in Tables 4 and 5, respectively. No significant inter- and intra-scanner differences for both parameters of all measured ten areas ($P > 0.05$).

4. Discussion

In the present study, the test-retest reproducibility and multi-site variability of ihMT in measuring major white matter fibers were evaluated. Good test-retest reproducibility and multi-site agreements were obtained.

Derived from conventional magnetization transfer, ihMT has been shown to be a promising method for myelin imaging in recent studies [26,27]. Conventional MT is sensitive to tissue macromolecular content by saturating the macromolecular proton pool and subsequent saturation transfer to the detectable mobile proton signal. Inhomogeneous MT, on the other hand, exploits the signal differences between single-frequency magnetic transfer RF saturation and two-symmetric-frequency magnetic transfer RF saturation. The signal difference can then be used to map the dipolar order underlying broad tissue macromolecular lines. The fact that myelinated structures have longer dipolar relaxation time compared with other tissues enables the ihMT with higher specificity for myelinated structures [28]. In this study, the

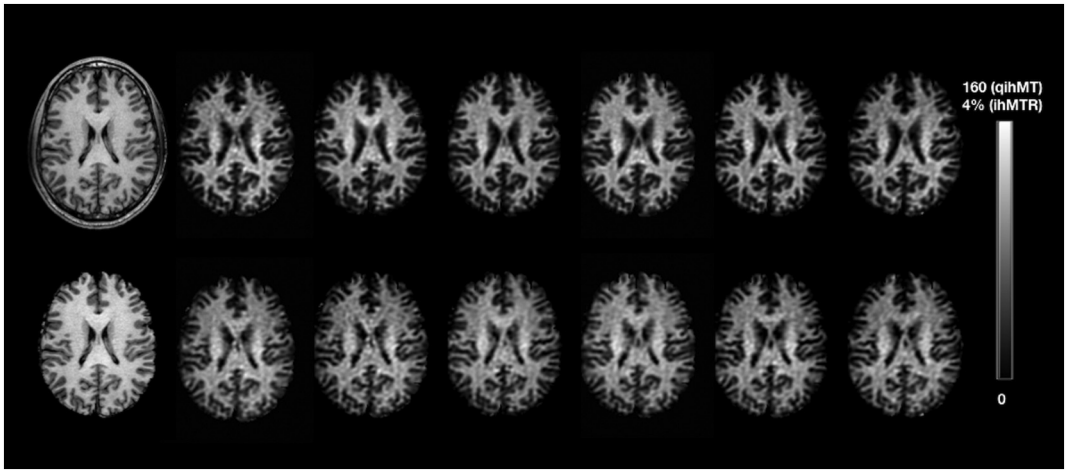

Fig. 2. Typical axial T1 anatomical without (top left) and with (bottom left) skull removal. The rest images in top row are spatially aligned axial qihMT images of a subject from different scans, including two scans from each of the three sites, while the images in bottom row are corresponding ihMTR maps. Gray bar for qihMT and ihMTR is illustrated on the right. All qihMT as well as ihMTR images were processed with skull removal for better display.

Table 1
qihMT values of ten areas from two tests in three scanners.

Area	Scanner 1		Scanner 2		Scanner 3	
	Test1	Test2	Test1	Test2	Test1	Test2
Genu of corpus callosum	81.39 ± 4.81	81.75 ± 5.41	80.42 ± 6.26	81.17 ± 5.33	82.25 ± 3.31	81.39 ± 3.46
Body of corpus callosum	81.74 ± 5.00	86.39 ± 8.23	87.88 ± 7.55	84.90 ± 6.09	83.88 ± 8.89	85.64 ± 9.38
Splenium of corpus callosum	85.21 ± 3.99	85.71 ± 6.24	86.24 ± 2.66	84.09 ± 5.83	84.94 ± 5.05	85.56 ± 6.47
Corticospinal tract	85.87 ± 3.26	87.34 ± 2.73	84.42 ± 1.45	86.15 ± 2.50	87.34 ± 4.43	85.09 ± 3.40
Cerebral peduncle	87.37 ± 4.41	89.40 ± 6.03	85.45 ± 4.99	88.81 ± 5.14	89.95 ± 4.40	87.10 ± 6.81
Limb of internal capsule	85.05 ± 4.48	86.29 ± 3.82	87.78 ± 8.42	88.61 ± 7.53	87.36 ± 2.58	84.00 ± 3.66
Corona radiata	94.42 ± 5.54	95.99 ± 5.41	95.71 ± 4.77	96.18 ± 3.49	96.08 ± 2.87	95.20 ± 3.82
Posterior thalamic radiation	92.19 ± 4.13	91.06 ± 6.10	90.86 ± 5.67	89.91 ± 6.49	94.30 ± 5.33	95.61 ± 6.11
Cingulate gyrus	86.36 ± 4.34	85.91 ± 2.83	85.40 ± 1.96	87.43 ± 3.90	86.87 ± 4.03	88.59 ± 3.96
Hippocampus	80.76 ± 10.10	83.67 ± 8.59	80.46 ± 7.72	80.84 ± 5.60	77.84 ± 9.20	78.14 ± 11.39

Table 2
ihMTR values (in 100 × %) of ten areas from two tests in three scanners.

Area	Scanner 1		Scanner 2		Scanner 3	
	Test1	Test2	Test1	Test2	Test1	Test2
Genu of corpus callosum	217.11 ± 13.12	215.63 ± 12.77	217.62 ± 17.31	221.04 ± 20.82	217.26 ± 16.25	217.29 ± 10.66
Body of corpus callosum	222.68 ± 24.26	228.96 ± 23.32	240.06 ± 16.46	229.15 ± 18.76	218.79 ± 19.74	224.86 ± 15.73
Splenium of corpus callosum	228.49 ± 12.09	223.22 ± 21.44	237.44 ± 15.27	231.85 ± 20.04	220.88 ± 13.74	229.37 ± 12.65
Corticospinal tract	243.00 ± 6.08	241.05 ± 10.43	238.84 ± 6.67	242.92 ± 9.89	242.65 ± 12.26	237.38 ± 16.41
Cerebral peduncle	247.75 ± 6.16	244.59 ± 12.52	245.07 ± 13.18	247.17 ± 15.84	245.99 ± 14.98	240.16 ± 24.68
Limb of internal capsule	227.83 ± 9.41	224.22 ± 10.95	232.31 ± 18.34	230.49 ± 19.63	229.01 ± 13.72	217.62 ± 11.70
Corona radiata	239.16 ± 7.89	238.53 ± 8.21	237.81 ± 14.24	234.57 ± 11.32	238.81 ± 12.21	233.79 ± 11.44
Posterior thalamic radiation	238.40 ± 8.22	233.98 ± 9.06	231.68 ± 15.51	232.91 ± 12.00	231.88 ± 10.12	234.20 ± 12.91
Cingulate gyrus	227.88 ± 9.05	225.63 ± 7.90	220.43 ± 12.48	223.12 ± 13.17	218.45 ± 16.42	232.79 ± 16.26
Hippocampus	214.21 ± 26.32	228.78 ± 23.78	216.25 ± 16.53	213.25 ± 13.91	206.43 ± 23.60	208.17 ± 26.98

Table 3
ICC results of qihMT and ihMTR for inter- and intra-scanner.

Area	Intra-scanner		Inter-scanner (1st–2nd scanner)		Inter-scanner (1st–3rd scanner)		Inter-scanner (2nd–3rd scanner)	
	qihMT	ihMTR	qihMT	ihMTR	qihMT	ihMTR	qihMT	ihMTR
Genu of corpus callosum	0.835	0.949	0.897	0.937	0.785	0.910	0.852	0.863
Body of corpus callosum	0.893	0.876	0.826	0.815	0.897	0.882	0.935	0.781
Splenium of corpus callosum	0.863	0.793	0.875	0.905	0.848	0.780	0.855	0.821
Corticospinal tract	0.776	0.761	0.812	0.739	0.836	0.877	0.714	0.787
Cerebral peduncle	0.841	0.825	0.874	0.766	0.754	0.786	0.794	0.747
Limb of internal capsule	0.870	0.792	0.796	0.774	0.718	0.791	0.693	0.818
Corona radiata	0.894	0.817	0.795	0.800	0.758	0.724	0.745	0.711
Posterior thalamic radiation	0.849	0.750	0.780	0.748	0.948	0.853	0.775	0.863
Cingulate gyrus	0.887	0.747	0.748	0.836	0.850	0.860	0.867	0.890
Hippocampus	0.924	0.832	0.779	0.795	0.863	0.871	0.850	0.762

qihMT values for major fiber tracts are in line with those reported in previous studies [21]: mean qihMT of Corpus Callosum Genu 84.5 1/ms and Corpus Callosum Body 87.60 1/ms. However, the ihMTR values measured in this study were lower than reported value [19]. For example, the ihMTR of corpus callosum observed in our study was around 2–3%, whereas Varma et al. reported that ihMTR varied in the range of 1%–6% depending on different set of saturation parameters. This difference is hypothesized to be due to the difference in saturation pulse length: saturation preparations in Varma's report were of hundreds of milliseconds (with fast spin echo readout); whereas the MT pulse used in this study was about 5 ms (with gradient echo readout). Varma also reported elevated ihMTR with lengthened MT saturation, especially when the saturation time is in the range of 0–200 ms.

Several reproducibility studies have been reported on myelin imaging techniques to date. Sandra et al. reported a 0.76 ICC for T2 based myelin water fraction imaging [22]. Magnetization transfer imaging was reported to have ICCs ranging from 0.572 to 0.962 in different brain region of interest [29]. In this study, inter-scanner ICCs were found to be higher than 0.693 in both qihMT and ihMTR for all ten measured tracts. In Mchinda's study, the standard deviations of inter-individual ihMTR were reported to be lower than 10% [25], which agreed with our findings. Intra-scanner ICCs in our study range from 0.776 to 0.924 for qihMT, and 0.747 to 0.949 for ihMTR. The Bland–Altman plots showed no bias of one scan over the other. In general, these plots revealed good agreement inter- and intra-scanners, showing only a small discrepancy between measurements. The evenly spread of points around zero showed that the bias level is independent of the numerical ranges, which indicates robustness of ihMT measurements for different levels of myelinations. To the best of our knowledge, the present study is the first to assess the multi-center reproducibility and test-retest variability of ihMT on 3.0 T systems.

The ihMT results can be affected by many parameters, including total saturation time, saturation RF energy and inter-pulse interval. Those parameters can be optimized to form a better image quality for a given acquisition sequence [26]. In this study, in order to achieve whole brain coverage in a clinical acceptable imaging time, 3D FSPGR fast

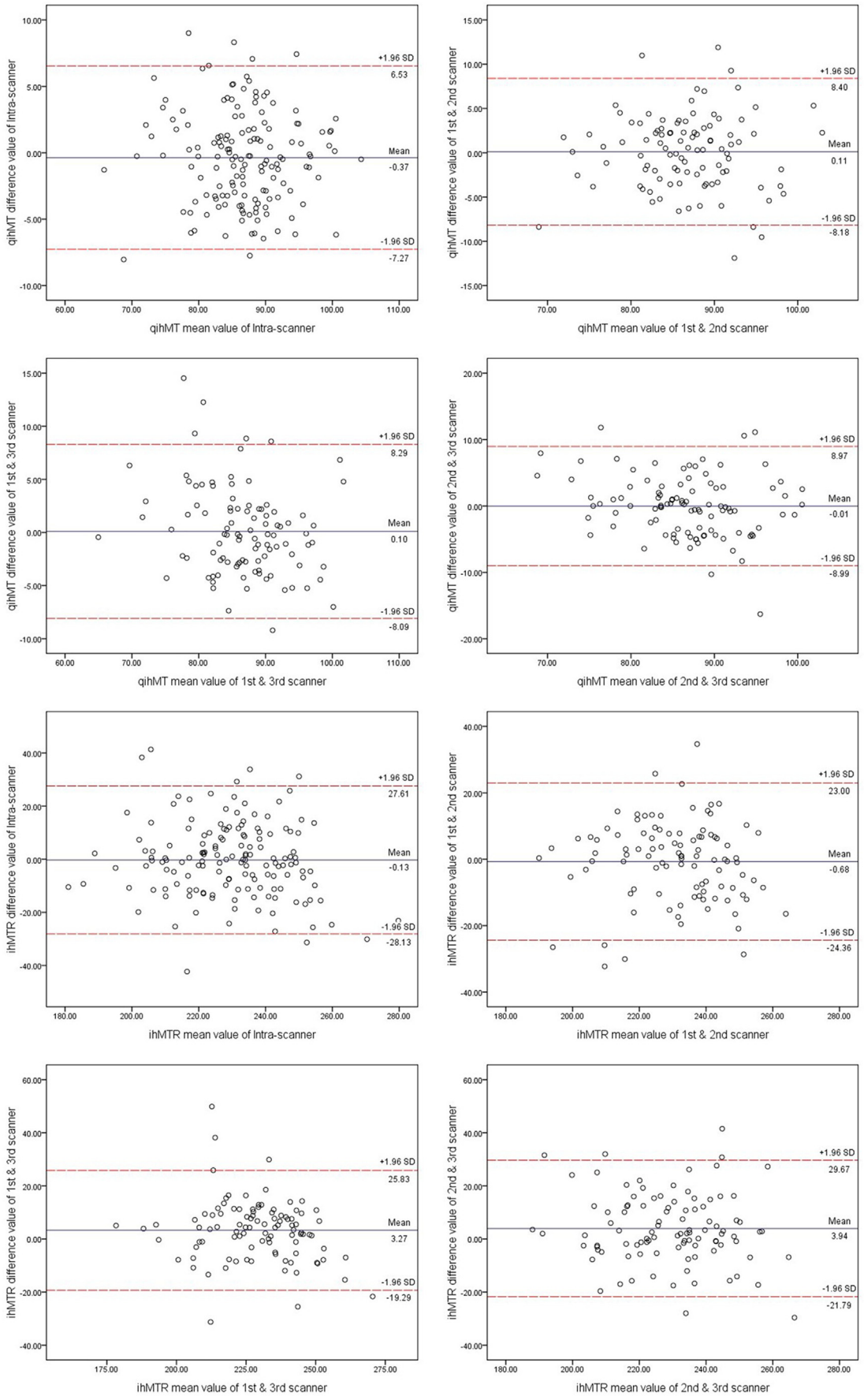

(caption on next page)

Fig. 3. Bland-Altman plots with 95% CI comparing the measurements of the intra- and inter-scanner to estimate the repeatability of qihMT and ihMTR in five volunteers. The mean differences between intra- and inter-scanner measurements (y-axis) are plotted against the averages of them (x-axis). The horizontal lines (solid line) are drawn at the mean difference of intra- and inter-scanner measurements and at the limits of agreement (dotted lines). The qihMT and ihMTR showed good accordance measurements of intra- and inter-scanner.

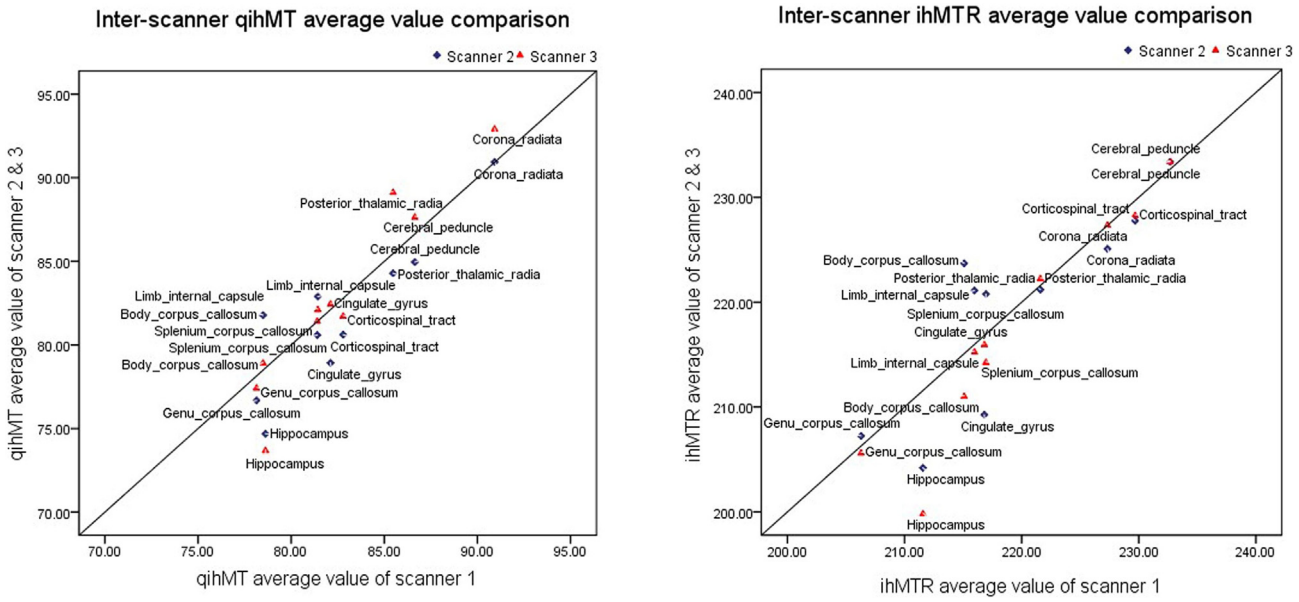

Fig. 4. Average qihMT and ihMTR value of 10 white matter areas from the five subjects on three MR scanners. The solid lines represent lines of unity. The qihMT and ihMTR showed good accordance measurements of interscanners.

Table 4
Comparison of qihMT and ihMTR values between test and retest.

Area	qihMT		ihMTR	
	t	*P* value	*t*	*P* value
Genu of corpus callosum	0.095	0.926	0.396	0.689
Body of corpus callosum	0.967	0.350	0.087	0.932
Splenium of corpus callosum	0.389	0.703	0.228	0.823
Corticospinal tract	0.459	0.653	0.447	0.662
Cerebral peduncle	0.854	0.408	0.871	0.398
Limb of internal capsule	0.458	0.654	2.027	0.062
Corona radiata	0.083	0.935	1.494	0.157
Posterior thalamic radiation	0.240	0.814	0.113	0.911
Cingulate gyrus	1.925	0.075	1.931	0.074
Hippocampus	1.029	0.321	1.033	0.319

Table 5
Comparison of qihMT and ihMTR values among three scanners.

Area	qihMT		ihMTR	
	F	*P* value	*F*	*P* value
Genu of corpus callosum	0.133	0.876	0.107	0.899
Body of corpus callosum	0.255	0.776	1.197	0.318
Splenium of corpus callosum	0.023	0.978	1.134	0.337
Corticospinal tract	0.486	0.621	0.093	0.911
Cerebral peduncle	0.210	0.812	0.143	0.867
Limb of internal capsule	0.749	0.483	0.849	0.439
Corona radiata	0.015	0.986	0.145	0.866
Posterior thalamic radiation	1.922	0.166	0.352	0.706
Cingulate gyrus	0.593	0.560	0.401	0.673
Hippocampus	0.609	0.551	1.080	0.354

sequence is used for data acquisition. Since ihMT use image subtraction in its post processing, which deteriorates the resulting SNR and vulnerability to motion. Careful trade-offs between image quality and scan time is important. The scan parameters used in this study were consistent with those used in a previous study [21]. Orientation dependency of ihMT imaging has been recently reported [30]. To minimize the impact of subject orientation variations in different measurements, all subjects were carefully positioned in every examination. The receive brain coil is fixed on the table at same position using a hold-down groove. All subjects lied down with head-first-spine posture and landmarks were positioned between the eyebrows. The body of the subjects is adjusted parallel to main magnetic field before examination.

The recent report from Manning et al. [31] suggested that ihMT signal originated from dipolar couplings alone and questioned the myelin specificity of ihMT measures. However, myelin specificity of ihMT was found to be higher when compared to with DTI and mcDESPOT [21]. A recent study validated ihMT as a biomarker for myelin by demonstrating linear relationships between ihMT signal and intensity of fluorescence microscopy (a quantitative myelin specific histology technique) in mouse brain [32]. In another bovine spinal cord study, specificity and sensitivity of ihMT were also histologically validated [33]. One possible explanation would be myelin is the only, or at least major, structure in CNS that possesses dipolar couplings.

There were several limitations in this work. Firstly, this study was performed with a small group of healthy volunteers with a narrow age range. Studies with a larger sample size, and subjects with a larger level of myelination variations such as patients with demyelination and elderly individuals are desired. Secondly, the ihMT spatial resolution is limited, mainly due to the desired whole brain coverage. The current spatial resolution ($2.4 \times 2.4 \times 3.2$ mm) may lead to partial volume effects and limit evaluation of small tracts. Higher channel phase array coils with improved signal-to-noise ratio, optimized fast sequence could help to improve spatial resolution. Thirdly, only one set of ihMT saturation strategy was used in this study, whereas it is desirable to assess the reproducibility of different ihMR settings.

In conclusion, good inter- and intra-scanner reliability and reproducibility of ihMT measurements were observed in this study. These findings support the use of ihMT measurements as biomarkers in multicenter and/or longitudinal studies.

Acknowledgement

We acknowledge Dr. Xiaocheng Wei from MR Research, GE Healthcare for technical support on ihMT sequence as well as helpful discussions.

Funding

The research did not receive any specific rant from funding agencies in the public, commercial, or not-for-profit sectors.

Declarations of interest

None.

References

[1] Boullerne Anne Isabelle. The history of myelin. Exp Neurol 2016;283(Pt B):431–45.
[2] Laule C, Vavasour IM, Moore GRW, Oger J, Li DKB, Paty DW, et al. Water content and myelin water fraction in multiple sclerosis. A T2 relaxation study. J Neurol 2004;251:284–93.
[3] Neema M, Goldberg-Zimring D, Guss ZD, Healy BC, Guttmann CRG, Houtchens MK, et al. 3 T MRI relaxometry detects T2 prolongation in the cerebral normal appearing white matter in multiple sclerosis. Neuroimage 2009;46:633–41.
[4] Sirrs S, Laule C, Madler B, Brief E, Tahir S, Bishop C, et al. Normal appearing white matter in patients with phenylketonuria: water content, myelin water fraction, and metabolite concentrations. Radiology 2007;242:236–43.
[5] Vermathen P, Robert-Tissot L, Pietz J, Lutz T, Boesch C, Kreis R. Characterization of white matter alterations in phenylketonuria by magnetic resonance relaxometry and diffusion tensor imaging. Magn Reson Med 2007;58:1145–56.
[6] Flynn S, Lang D, Mackay A, Goghari V, Vavasour I, Whittall K, et al. Abnormalities of myelination in schizophrenia detected in-vivo with MRI, and postmortem with analysis of oligodendrocyte proteins. Mol Psychiatry 2003;8:811–20.
[7] Jackson GD, Connelly A, Duncan JS, Grunewald RA, Gadian DG. Detection of hippocampal pathology in intractable partial epilepsy: increased sensitivity with quantitative magnetic resonance T2 relaxometry. Neurology 1993;43:1793–9.
[8] Wood SJ, Cocchi L, Proffitt TM, McConchie M, Jackson GD, Takahashia T, et al. Neuroprotective effects of ethyl-eicosapentaenoic acid in first episode psychosis: a longitudinal T2 relaxometry pilot study. Psychiatry Res 2010;182:180–2.
[9] Bartzokis G, Lu PH, Mintz J. Quantifying age-related myelin breakdown with MRI: novel therapeutic targets for preventing cognitive decline and Alzheimer's disease. J Alzheimers Dis 2004;6:S53–9.
[10] Whitaker K, Kolind S, MacKay A, Clark C. Quantifying development: investigating highly myelinated voxels in preadolescent corpus callosum. Neuroimage 2008;43:731–5.
[11] Gulani V, Webb A, Duncan I, Lauterbur P. Apparent diffusion tensor measurements in myelin-deficient rat spinal cords. Magn Reson Med 2001;45:191–5.
[12] Beaulieu C. The biological basis of diffusion anisotropy. In: Johansen-Berg H, Behrens TE, editors. Diffusion MRI: from quantitative measurement to in vivo neuroanatomy, chapter 6. London: Elsevier; 2009. p. 105–26.
[13] Deoni SCL, Rutt BK, Arun T, Pierpaoli C, Jones DK. Gleaning multicomponent T1 and T2 information from steady-state imaging data. Magn Reson Med 2008;60:1372–87.
[14] Lenz C, Klarhofer M, Scheffler K. Limitations of rapid myelin water quantification using 3D bSSFP. MAGMA 2010;23:139–51.
[15] Deloire-Grassin MS, Brochet B, Quesson B, Delalande C, Dousset V, Canioni P, et al. In vivo evaluation of remyelination in rat brain by magnetization transfer imaging. J Neurol Sci 2000;178:10–6.
[16] Schmierer K, Tozer DJ, Scaravilli F, Altmann DR, Barker GJ, Tofts PS, et al. Quantitative magnetization transfer imaging in postmortem multiple sclerosis brain. J Magn Reson Imaging 2007;26:41–51.
[17] Gareau PJ, Rutt BK, Karlik SJ, Mitchell JR. Magnetization transfer and multicomponent T2 relaxation measurements with histopathologic correlation in an experimental model of MS. Magn Reson Imaging 2000;11:586–95.
[18] Henkelman RM, Huang X, Xiang Q-S, Stanisz GJ, Swanson SD, Bronskill MJ. Quantitative interpretation of magnetization transfer. Magn Reson Med 1993;29:759–66.
[19] Varma G, Duhamel G, de Bazelaire C, Alsop DC. Magnetization transfer from inhomogeneously broadened lines: a potential marker for myelin. Magn Reson Med 2015;73:614–22.
[20] Girard OM, Callot V, Prevost VH, et al. Magnetization transfer from inhomogeneously broadened lines (ihMT): improved imaging strategy for spinal cord applications. Magn Reson Med 2017;77:581–91.
[21] Geeraert BL, Lebel RM, Mah AC, Deoni SC, Alsop DC, Varma G, et al. A comparison of inhomogeneous magnetization transfer, myelin volume fraction, and diffusion tensor imaging measures in healthy children. Neuroimage 2017. https://doi.org/10.1016/j.neuroimage.2017.09.019.
[22] Meyers SM, Vavasour IM, Mädler B, Harris T, Fu E, Li DK, et al. Multicenter measurements of myelin water fraction and geometric mean T2: intra- and intersite reproducibility. J Magn Reson Imaging 2013;38:1445–53.
[23] Arshad M, Stanley JA, Raz N. Test – retest reliability and concurrent validity of in vivo myelin content indices: myelin water fraction and calibrated T1w/T2w image ratio. Hum Brain Mapp 2017;38(4):1780–90. https://doi.org/10.1002/hbm.23481.
[24] Levesque IR, Chia CL, Pike GB. Reproducibility of in vivo magnetic resonance imaging-based measurement of myelin water. J Magn Reson Imaging 2010;32:60–8.
[25] Mchinda S, Varma G, Prevost VH, et al. Whole brain inhomogeneous magnetization transfer (ihMT) imaging: sensitivity enhancement within a steady-state gradient echo sequence. Magn Reson Med 2018;79(5). https://doi.org/10.1002/mrm.26907.
[26] Girard OM, Prevost VH, Varma G, Cozzone PJ, Alsop DC, Duhamel G. Magnetization transfer from inhomogeneously broadened lines (ihMT): experimental optimization of saturation parameters for human brain imaging at 1.5 Tesla. Magn Reson Med 2015;73:2111–21.
[27] Girard OM, Callot V, Prevost VH, Robert B, Taso M, Ribeiro G, et al. Magnetization transfer from inhomogeneously broadened lines (ihMT): improved imaging strategy for spinal cord applications. Magn Reson Med 2017;77:581–91.
[28] Varma G, Girard OM, Prevost VH, et al. In vivo measurement of a new source of contrast, the dipolar relaxation time, T1D, using a modified inhomogeneous magnetization transfer (ihMT) sequence. Magn Reson Med 2017;78:1362–72.
[29] Zou KH, Du H, Sidharthan S, et al. Statistical evaluations of the reproducibility and reliability of 3-tesla high resolution magnetization transfer brain images: a pilot study on healthy subjects. Int J Biomed Imaging 2010:618747.
[30] Manning AP, Frederick RE, MacKay AL, Michal CA. Exploring the ihMT dependence on dipolar coupling using oriented lipid bilayers. ISMRM workshop - quantitative MRI in white matter disorders: useful, usable, used?, Vancouver, Canada. 2017. p. 064.
[31] Manning AP, Chang KL, MacKay AL, Michal CA. The physical mechanism of "inhomogeneous" magnetization transfer MRI. J Magn Reson 2017;274:125–36.
[32] Prevost VH, Girard OM, Cayre M, Varma G, Mchinda S, Ranjeva JP, et al. Validation of inhomogeneous magnetization transfer (ihM)T as a myelin biomarker. ISMRM Annual Meeting, Hawaii. 2017. p. 4549.
[33] Swanson SD, Malyarenko DI, Fabiilli ML, Welsh RC, Nielsen JF, Srinivasan A. Molecular, dynamic, and structural origin of inhomogeneous magnetization transfer in lipid membranes. Magn Reson Med 2017;77:1318–28.